ORIGINAL ARTICLE

Benefits of BDS-3 B1C/B1I/B2a triple-frequency signals on precise positioning and ambiguity resolution

Jinlong Li[1] · Yuanxi Yang[2] · Haibo He[1] · Hairong Guo[1]

Abstract

BDS-3 currently has 28 operational satellites in orbit, of which 27 IGSO/MEO satellites provide open services on five frequencies simultaneously. In particular, the linear combinations of the BDS-3 B1C/B1I/B2a signals have significant benefits in reducing the influence of ionospheric delay error as well as improving ambiguity estimation and positioning accuracy. The presented optimal ionosphere-free combination (242, 218, −345) and ionosphere-reduced combination (2, 2, −3) can improve the measurement accuracy by about 20% compared to the BDS-3 B1C/B2a or GPS L1/L5 dual-frequency combination. The ionosphere-reduced combination (2, 2, −3) with a wavelength of 10.9 cm is almost immune to the ionospheric delay error and has a smaller noise amplification factor compared to the existing dual-frequency combinations. Therefore, its combined ambiguities can be fixed directly even in the case of a long baseline, which can simplify the traditional precise positioning process based on the ionosphere-free combination. The numerical results of BDS-3 real data show that the triple-frequency ionosphere-free or ionosphere-reduced combinations can improve the single-point positioning accuracy by 16–20% and the phase differential positioning accuracy by 7–9%, respectively. The ambiguity resolution of the ionosphere-reduced combination (2, 2, −3) is achieved with a fixing rate of 88.4% over long baseline up to 1600 km. The presented ionosphere-free and ionosphere-reduced combinations are also very promising to be applied in current PPP applications to simplify the ambiguity fixing process as well as improve positioning accuracy and shorten convergence time.

Keywords BDS-3 · Linear combination · Long baseline · Ambiguity resolution · Positioning accuracy

Introduction

The BDS-3 basic system with 18 MEO satellites has started to provide initial global services on December 27, 2018 (Yang et al. 2020b), and it is expected to provide full operational capability services by June 2020. At present (March 24, 2020), there are a total of 29 BDS-3 satellites in orbit, including 24 medium earth orbit (MEO) satellites, 3 Inclined Geo-Synchronous Orbit (IGSO) satellites and 2 geostationary earth orbit (GEO) satellites. Except for the GEO satellite launched on March 9, which is undergoing in-orbit testing, the remaining 28 satellites have been providing operational services, of which 24 MEO satellites and 3 IGSO satellites

broadcast open service signals simultaneously on five frequencies including 1575.42 MHz (B1C), 1561.098 MHz (B1I), 1268.52 MHz (B3I), 1207.14 MHz (B2b) and 1176.45 MHz (B2a) (Yang et al. 2019). The comparison of the BDS-3, GPS, GLONASS (CDMA signals only) and Galileo open service signals is shown in Table 1 (RNSS: Radio Navigation Satellite Services, ARNS: Aeronautical Radio Navigation Services).

As given in Table 1, the common points of the frequency selection of each GNSS signals are: (1) they can be divided into three categories, namely upper L-band/ARNS band, lower L-band/RNSS band and lower L-band/ARNS band; and (2) there is only one frequency in the lower L-band/RNSS band. The differences are: (1) in the upper L-band/ARNS band, GPS, GLONASS and Galileo only have one frequency, while BDS-3 has two frequencies; (2) in the lower L-band/ARNS band, GPS and GLONASS have only one frequency, while BDS-3 and Galileo both have two frequencies. BDS-3 is currently the satellite navigation system with the most navigation signals and the most frequency

✉ Jinlong Li
   along0730@163.com

1. Beijing Satellite Navigation Center, Beijing 100094, China

2. National Key Laboratory of Geo-Information Engineering, Xi'an 710054, China

Table 1 BDS-3, GPS, GLONASS and Galileo open service signals (RTCM-SC104 2018)

GNSS	Signal	Frequency (MHz)	Frequency band
GLONASS	G1a	1600.995	Upper L-band/ARNS band
BDS-3, GPS, Galileo	B1C, L1C/A and L1C, E1	1575.42	
BDS-2 and BDS-3	B1I	1561.098	
Galileo	E6	1278.75	Lower L-band/RNSS band
BDS-2 and BDS-3	B3I	1268.52	
GLONASS	G2a	1248.06	
GPS	L2C	1227.60	
BDS-3 (BDS-2), Galileo	B2b(B2I), E5b	1207.14	Lower L-band/ARNS band
GLONASS	G3	1202.025	
BDS-3, GPS, Galileo	B2a, L5, E5a	1176.45	

diversity. The diversity of frequencies can improve anti-jamming capability (Hatch et al. 2000), cycle slip detection (Blewitt 1990; Zhao et al. 2015; Zhang and Li 2016; Li et al. 2019), ambiguity resolution (AR) performance (Han and Rizos 1999; Hatch 2006; Simsky 2006; Feng 2008; Li et al. 2014, 2015) and positioning accuracy (Richert and El-Sheimy 2007). The multi-frequency linear combination can also eliminate or mitigate errors, alleviate computational burdens and reduce communication bandwidth (Richert and El-Sheimy 2007).

The triple-frequency linear combination has been widely studied in the literature, and the three frequencies used are generally one upper L-band and two lower L-bands, such as GPS L1/L2/L5 (Cocard et al. 2008) and BDS-2 B1I/B3I/B2I (two ARNS bands and one RNSS band) (Li et al. 2012; Zhang and He 2015) and Galileo E1/E5b/E5a (three ARNS bands). However, BDS-3 has a special triple-frequency selection, that is, two upper L-bands and one lower L-band, such as B1C/B1I/B3I (two ARNS bands and one RNSS band), B1C/B1I/B2b and B1C/B1I/B2a (three ARNS bands), which have not been treated in detail until now. In particular, the triple-frequency case of the B1C/B1I/B2a signals has a larger frequency interval, which is beneficial to mitigate ionospheric delay as well as improve ambiguity estimation and positioning accuracy (Hatch et al. 2000; Hatch 2006).

In this contribution, the optimal geometry-free (GF), ionosphere-free (IF) and ionosphere-reduced (IR) linear combinations for the B1C/B1I/B2a signals are presented first, followed by a direct AR strategy over long baseline based on the optimal IR combinations. The benefits of the B1C/B1I/B2a triple-frequency linear combinations on precise positioning and ambiguity estimation are validated by the single-point positioning and kinematic differential positioning experiment.

Optimal B1C/B1I/B2a linear combinations

The original carrier phase and code observations can be expressed as:

$$\varphi_j = \frac{f_j}{c}\rho - \kappa_j d_{\text{ion}} + n_j + v_j \tag{1a}$$

$$\phi_j = \lambda_j \varphi_j = \rho - \mu_j d_{\text{ion}} + b_j + \varepsilon_j \tag{1b}$$

$$p_j = \rho - \mu_j d_{\text{ion}} + d_j + e_j \tag{1c}$$

where j is the frequency identifier ($j = 1, 2, 3$), φ_j and ϕ_j are the carrier phase observation in cycles and distance, respectively, p_j is the code observation, f_j is the fth frequency, c is the velocity of light in vacuum and ρ is the frequency-independent term including the satellite–receiver geometric distance, satellite and receiver clock errors, and tropospheric delay. $\kappa_j = \frac{f_1^2}{c f_j}$ is a frequency-dependent amplification factor, d_{ion} is the first-order ionospheric delay on the first frequency, and n_j is the sum of the initial phase, the phase ambiguity and the instrumental phase delay. v_j is the unmodeled phase observation error, including carrier phase measurement noise, multi-path error and high-order ionospheric delay error. $\lambda_j = \frac{c}{f_j}$ is the wavelength of the jth frequency. Further, $\mu_j = \lambda_j \kappa_j = \frac{f_1^2}{f_j^2}$, $b_j = \lambda_j n_j$, and $\varepsilon_j = \lambda_j v_j$. d_j is the instrumental code delay, and e_j is the unmodeled code observation error, which includes code measurement noise, multi-path errors and high-order ionospheric delay errors.

The triple-frequency carrier phase and code linear combinations can be expressed as (Cocard et al. 2008; Feng 2008; Li 2014):

$$\varphi_{(i,j,k)} = i \cdot \varphi_1 + j \cdot \varphi_2 + k \cdot \varphi_3 = \frac{f_{(i,j,k)}}{c} \rho - \kappa_{(i,j,k)} d_{\text{ion}} + n_{(i,j,k)} + v_{(i,j,k)}$$
(2a)

$$\phi_{\langle i,j,k \rangle} = \frac{c}{f_{(i,j,k)}} \varphi_{(i,j,k)} = \frac{i \cdot f_1 \cdot \phi_1 + j \cdot f_2 \cdot \phi_2 + k \cdot f_3 \cdot \phi_3}{i \cdot f_1 + j \cdot f_2 + k \cdot f_3} = \rho - \mu_{\langle i,j,k \rangle} d_{\text{ion}} + b_{\langle i,j,k \rangle} + \varepsilon_{\langle i,j,k \rangle}$$
(2b)

$$p_{\langle i,j,k \rangle} = \frac{i \cdot f_1 \cdot p_1 + j \cdot f_2 \cdot p_2 + k \cdot f_3 \cdot p_3}{i \cdot f_1 + j \cdot f_2 + k \cdot f_3} = \rho + \mu_{\langle i,j,k \rangle} d_{\text{ion}} + d_{\langle i,j,k \rangle} + e_{\langle i,j,k \rangle}$$
(2c)

where the subscript notation means $()_{(i,j,k)} = i \cdot ()_1 + j \cdot ()_2 + k \cdot ()_3$ and $()_{\langle i,j,k \rangle} = \frac{i \cdot f_1 \cdot ()_1 + j \cdot f_2 \cdot ()_2 + k \cdot f_3 \cdot ()_3}{i \cdot f_1 + j \cdot f_2 + k \cdot f_3}$. For example, $\kappa_{(i,j,k)} = i \cdot \kappa_1 + j \cdot \kappa_2 + k \cdot \kappa_3$ and $\mu_{\langle i,j,k \rangle} = \frac{i \cdot f_1 \cdot \mu_1 + j \cdot f_2 \cdot \mu_2 + k \cdot f_3 \cdot \mu_3}{i \cdot f_1 + j \cdot f_2 + k \cdot f_3}$. Finally, $\lambda_c = \frac{c}{f_{(i,j,k)}}$ is the virtual wavelength of the triple-frequency linear combination.

Considering the B1C/B1I/B2a triple-frequency case, and taking $f_1 = 1575.42$ MHz (B1C), $f_2 = 1561.098$ MHz (B1I) and $f_3 = 1176.45$ MHz (B2a) into account, we can get the optimal GF, IF and IR combinations for cycle slip detection, precise positioning and ambiguity estimation, following the method presented in Li et al. (2017). We make use of the following notation: $\eta = \sqrt{i^2 + j^2 + k^2}$ is the combined noise amplification factor, $w = \frac{\sqrt{(i \cdot f_1)^2 + (j \cdot f_2)^2 + (k \cdot f_3)^2}}{i \cdot f_1 + j \cdot f_2 + k \cdot f_3}$ is the noise amplification factor of the linear combination observations relative to the first frequency (B1C) observations, $s = i + j + k$ is the sum of integer linear coefficients, and $\gamma = \frac{\kappa_{(i,j,k)}}{\sqrt{2} \cdot \eta}$ is the factor quantifying the influence of the ignored ionospheric delay on the cycle slip detection using GF combinations (Li et al. 2017).

GF combinations

The GF linear combination, $f_{(i,j,k)} = 0$, eliminates the influence of frequency-independent term ρ and is generally used for data preprocessing such as cycle slip detection and measurement noise analysis. Table 2 shows the GF linear combinations for cycle slip detection. For comparison, the table also shows the commonly used dual-frequency GF combinations (also called the ionospheric residual combination).

As given in Table 2, the GF combination $(-30, 25, 7)$ has the strongest (η is smallest) cycle slip detection capability, followed by the combination $(79, -85, 7)$. When the ionospheric delay variation between epochs is less than 2 cm, and then the effect on the cycle slip is smaller than 0.01 cycle ($0.02 \times 0.4311 < 0.01$ cycle), these two GF combinations should be selected for cycle slip detection to minimize the number of insensitive cycle slip groups. The GF combinations $(79, -85, 7)$ and $(-109, 110, 0)$ can still be used when the ionospheric delay change between epochs reaches 0.1 m ($0.1 \times 0.0829 < 0.01$ cycle). The GF combination that is the least affected by the ionospheric delay is $(188, -195, 7)$ (called GFS0 combination Li et al. 2017), followed by the combination $(-297, 305, -7)$; these two combinations can still be used even if the ionospheric delay changes between epochs reach 0.8 m ($0.8 \times 0.0124 < 0.01$ cycle). The dual-frequency GF combinations, $(115, 0, -154)$ and $(0, 575, -763)$, usually cannot be used for cycle slip detection except if the ionospheric delay variation between epochs is less than 5 mm ($0.005 \times 1.7637 < 0.01$ cycle). Therefore, the triple-frequency GF combinations are better than the commonly used dual-frequency GF combination in terms of cycle slip detection capability and the impact of ionospheric delay reduction.

Table 2 GF combinations for cycle slip detection

i	j	k	s	$\kappa_{(i,j,k)}$	η	γ
-30	25	7	2	24.19	39.67	0.4311
79	-85	7	1	13.63	116.25	0.0829
-109	110	0	1	10.56	154.86	0.0482
115	0	-154	-39	-479.39	192.20	-1.7637
-139	135	7	3	34.75	193.89	0.1267
188	-195	7	0	3.07	270.96	0.0080
267	-280	14	1	16.71	387.15	0.0305
-297	305	-7	1	7.48	425.77	0.0124
346	-365	21	2	30.34	503.37	0.0426
-406	415	-7	2	18.04	580.61	0.0220
0	575	-763	-188	-2319.99	955.40	-1.7171

Table 3 Optimal IF combinations for precise positioning

Signals	i	j	k	s	λ_c (cm)	η	w	λ_e (cm)
B1C/L1	1	0	0	1	19.03	1.00	1.00	19.03
B1C/B1I/B2a	242	218	−345	115	0.09	474.46	2.07	10.92
	286	327	−460	153	0.07	632.71	2.07	10.92
	198	109	−230	77	0.14	322.47	2.11	10.91
	44	109	−115	38	0.29	164.44	2.19	10.93
	352	109	−345	116	0.09	504.79	2.22	10.91
	506	109	−460	155	0.07	692.47	2.30	10.90
	66	545	−460	151	0.07	716.23	2.45	10.94
	154	0	−115	39	0.28	192.20	2.59	10.89
	22	436	−345	113	0.10	556.42	2.56	10.95
	0	763	−575	188	0.06	955.40	2.66	10.95
	110	−109	0	1	9.56	154.86	77.43	9.56
	4136	−4251	115	0	1.99	5932.17	620.04	8265.58
GPS L1/L2/L5	77	−36	−23	18	0.60	88.06	2.64	10.78
	77	−12	−46	19	0.57	90.49	2.55	10.86
	154	−48	−69	37	0.29	175.45	2.56	10.82

IF combinations

The IF combinations ($\kappa_{(i,j,k)} = 0$, $\mu_{(i,j,k)} = 0$) eliminate the effect of first-order ionospheric delay and are generally used in cases of precise positioning and ambiguity estimation for long baselines. Table 3 shows the optimal IF combinations suitable for precise positioning, where λ_e is the effective wavelength of the IF combination in the case that the EWL or WL ambiguities are fixed in advance. The IF combination (4136, −4251, 115) is the so-called the IFS0 combination (Li et al. 2017). For comparison, the optimal IF combinations of GPS L1/L2/L5 frequencies are also presented in Table 3.

As given in Table 3, the noise amplification factors (w) for the most B1C/B1I/B2a triple-frequency IF combinations are evidently smaller than those of dual-frequency IF combinations, such as (242, 218, −345), (286, 327, −460) and (198, 109, −230). Compared to the B1C/B2a or L1/L5 dual-frequency IF combination (154, 0, −155), the improvement of the measurement accuracy is up to about 20.1% (2.07 vs 2.59). However, the GPS L1/L2/L5 triple-frequency IF combinations (154, −48, −69), (77, −12, −46) and (77, −36, −23) can only improve the measurement accuracy about 1.5% (2.55 vs 2.59) which is almost negligible relative to the dual-frequency IF combination (154, 0, −155). Considering that all these IF combinations have equivalent wavelengths λ_e (approximately 10.9 cm), so the B1C/B1I/B2a triple-frequency IF combinations with smaller measurement noise can not only improve the positioning accuracy but also improve the ambiguity estimation compared to the B1C/B2a or L1/L5 dual-frequency IF combinations.

IR combinations

The IR combinations are used for ambiguity estimation and precise positioning in the case of medium and long baselines. Table 4 shows the IR linear combinations with the sum of the linear coefficients equal to 1.

Table 4 shows that the optimal B1C/B1I/B2a IR combination is (2, 2, −3). Even if the ionospheric delay error reaches 10 m, its effect on AR is only 0.05 cycles and the effect on the corresponding positioning solution is only 5 mm. The next suboptimal IR combinations are (3, 1, −3) and (1, 3, −3). Compared to the BDS-3 B1C/B2a or GPS L1/L5 dual-frequency IR combination (4, 0, −3), the improvement in reducing the impact of the ionospheric delay is 18 times (0.0914/0.005 = 18.3) better, and the improvement in measurement accuracy is about 20.7%. Therefore, compared to the dual-frequency IR combination, the optimal triple-frequency IR combination of B1C/B1I/B2a can not only improve the precision positioning accuracy but also improve the ambiguity estimation. For the GPS L1/L2/L5 case, the optimal triple-frequency IR combination (4, −1, −2) only improves 3.8% in terms of measurement accuracy compared to the dual-frequency IR combination (4, 0, −3) and is more sensitive to the influence of ionospheric delay. This is shown again the advantage of the BDS-3 B1C/B1I/B2a signals in mitigating ionospheric delay as well as improving ambiguity estimation and positioning accuracy.

AR strategy based on optimal IR combinations

The optimal triple-frequency IR combinations have a very weak sensitivity to ionospheric delay errors. In addition,

Table 4 IR combinations with the sum of linear coefficients equal to 1

Signals	i	j	k	λ_c (cm)	$\kappa_{(i,j,k)}$	$\mu_{(i,j,k)}$	η	w
B1C/L1	1	0	0	19.03	5.2550	1.0000	1.00	1.00
B1C/B1I/B2a	−4	8	−3	11.28	0.2943	0.0332	9.43	5.43
	−3	7	−3	11.22	0.2461	0.0276	8.19	4.65
	−2	6	−3	11.16	0.1979	0.0221	7.00	3.91
	−1	5	−3	11.10	0.1497	0.0166	5.92	3.23
	0	4	−3	11.04	0.1015	0.0112	5.00	2.64
	1	3	−3	10.98	0.0532	0.0058	4.36	2.22
	2	2	−3	10.93	0.0050	0.0005	4.12	2.07
	3	1	−3	10.87	−0.0432	−0.0047	4.36	2.21
	4	0	−3	10.81	−0.0914	−0.0099	5.00	2.61
	5	−1	−3	10.76	−0.1396	−0.0150	5.92	3.15
	6	−2	−3	10.70	−0.1878	−0.0201	7.00	3.77
	7	−3	−3	10.65	−0.2360	−0.0251	8.19	4.44
	8	−4	−3	10.59	−0.2842	−0.0301	9.43	5.12
	−3	8	−4	9.81	−1.4878	−0.1459	9.43	4.63
GPS L1/L2/L5	4	−1	−2	11.02	0.2018	0.0222	4.58	2.51
	4	−2	−1	11.23	0.4950	0.0556	4.58	2.57

Table 5 Phase differential positioning methods based on the traditional IF combination and IR combination

Method	Data processing steps	Efficiency	Transmission data
Traditional phase differential positioning based on the IF combinations	1. Solve the float ambiguities of the IF combination 2. Using MW combination to solve the integer solution of wide-lane (WL) ambiguities 3. The narrow-lane (NL) ambiguities are derived from the integer WL ambiguities and the float IF ambiguities 4. Solve the integer solution of the NL ambiguities 5. Solve the fixed solution of the IF carrier phase observation	There are five steps in total	In the triple-frequency case, three code observations and three carrier phase observations are needed to be transmitted
Phase differential positioning based on the IR combinations	1. Solve the float ambiguities of the IR combination 2. Solve the float ambiguities to their integer values 3. Solve the fixed solution of the IR carrier phase observation	The steps (2) and (3) of the current process are reduced, so the calculation efficiency is improved	Only one IR code observation and one IR carrier phase observation are transmitted, reducing the communication bandwidth about 43% and 60% in dual- and triple-frequency case (RTCM-SC104 2013)

its wavelength is about 11 cm and it has a smaller noise amplification factor than the existing dual-frequency IF and IR combinations. Therefore, their combined ambiguities can be fixed directly for long baselines, which can simplify the current precise positioning process based on the IF combination (Blewitt 1989; Dong and Bock 1989; Odijk 2003) and improve positioning accuracy and AR performance. The comparisons with the phase differential positioning methods based on the traditional IF combination and IR combination are shown in Table 5.

Numerical experiments

From March 7 to 13, 2020, two test terminals were used to collect BDS-3 data at two stations in Urumqi and Lhasa, with a sampling interval of 30 s. The precise coordinates of the two stations were determined by carrier phase differential positioning (< 15 km) from two nearby IGS stations: URUM and LHAZ. All MEO and IGSO satellite (27 satellites, C19–C30, C32–C46) data are used in the
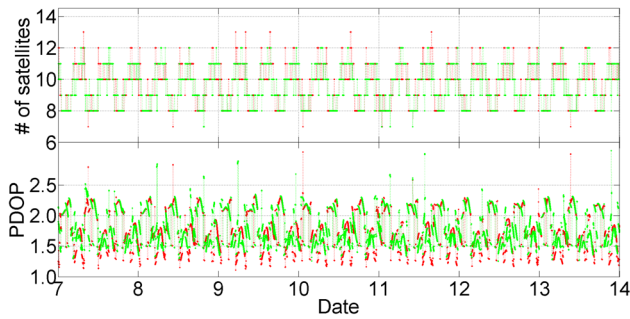
Fig. 1 Number of visible BDS-3 satellites and PDOP value (red: Urumqi, green: Lhasa)

experiment; the C59 (GEO) data were not used since it did not broadcast B1C and B2a signals. The number of visible BDS-3 satellites and PDOP value at the two stations are shown in Fig. 1. Seven to thirteen BDS-3 satellites can be observed during the test, with corresponding PDOP values between 1.1 and 2.5.

Single-point positioning

First, the single-point positioning experiment was performed to verify the absolute positioning improvement of the triple-frequency IF and IR combinations relative to the dual-frequency combination. In the experiment, the original B1C, B1I and B2a code observations were corrected by the group delay differential corrections, and then, the IF and IR linear combinations of them were used

to solve the single-point positioning solution. The ephemeris and clock correction parameters from the B-CNAV1 message of the B1C signal were used to calculate the satellite position and satellite clock errors, the tropospheric delay was corrected by the Saastamoinen model (Saastamoinen 1973), the ionospheric delay was eliminated or mitigated by the IF and IR combinations, and the cutoff angle was set to 5°.

Table 6 shows that the RMS statistics of single-point positioning for all triple-frequency IF and IR combinations are smaller to the corresponding dual-frequency combinations. Compared to the dual-frequency combination #8 and #14, the optimal triple-frequency IF combination #1 and IR combination #11 can improve the single-point positioning accuracy by 16–20%, and their positioning error for Urumqi station is shown in Figs. 2 and 3. In addition, the optimal
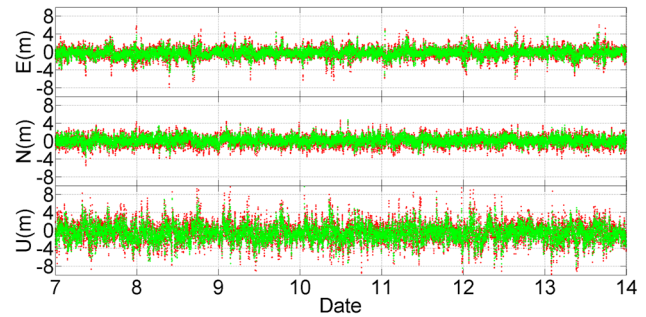

Fig. 2 Single-point positioning errors for both the dual- and triple-frequency IF combinations (red: #8, green: #1)

Table 6 RMS of single-point positioning with the IF and IR combinations (unit: m)

| Combination	Number	Linear coefficients			Urumqi			Lhasa		
					H	V	Position	H	V	Position
IF	#1	242	218	−345	1.24	1.83	2.21	1.32	2.54	2.86
	#2	286	327	−460	1.24	1.84	2.22	1.32	2.52	2.85
	#3	198	109	−230	1.27	1.86	2.25	1.35	2.62	2.95
	#4	44	109	−115	1.29	1.92	2.31	1.35	2.57	2.90
	#5	352	109	−345	1.33	1.93	2.35	1.41	2.75	3.09
	#6	506	109	−460	1.37	1.98	2.41	1.45	2.84	3.19
	#7	66	545	−460	1.41	2.09	2.53	1.45	2.76	3.12
	#8	154	0	−115	1.53	2.18	2.66	1.59	3.14	3.52
	#9	22	436	−345	1.47	2.17	2.62	1.50	2.86	3.23
	#10	0	763	−575	1.52	2.24	2.70	1.54	2.94	3.32
IR	#11	2	2	−3	1.24	1.83	2.21	1.32	2.53	2.85
	#12	3	1	−3	1.32	1.93	2.34	1.41	2.75	3.09
	#13	1	3	−3	1.30	1.94	2.33	1.36	2.59	2.92
	#14	4	0	−3	1.54	2.20	2.68	1.61	3.17	3.55
	#15	0	4	−3	1.51	2.22	2.68	1.53	2.91	3.29
Improvement #1 versus #8 (%)					18.9	15.9	16.8	16.9	19.3	18.8
Improvement #11 versus #14 (%)					19.5	16.5	17.5	17.8	20.2	19.7
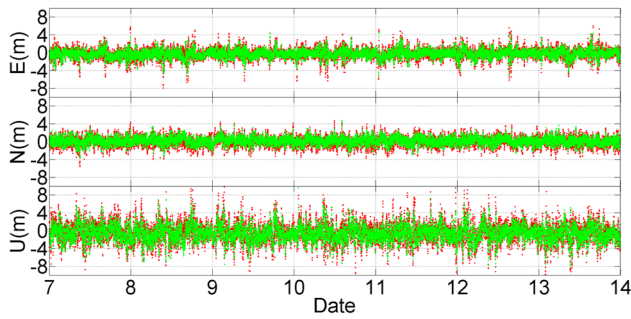
Fig. 3 Single-point positioning errors for dual- and triple-frequency IR combinations (red: #14, green: #11)
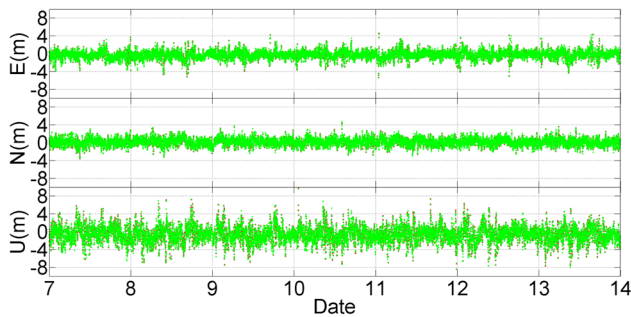

Fig. 4 Single-point positioning errors for triple-frequency IF and IR combinations (red: #1, green: #11)

triple-frequency IF combination #1 and IR combination #11 have almost the same positioning accuracy and highly overlapping error sequences (Fig. 4). The result demonstrates that even in the case of absolute positioning, the influence of the ionospheric delay error on the optimal triple-frequency IR combination can still be ignored, so they can also be used for high-precision absolute positioning applications, such as PPP positioning.

Kinematic differential positioning over long baseline

The baseline length between stations Urumqi and Lhasa is about 1600 km, and their geodetic heights are 900 m and 3600 m, respectively. The cutoff angle was 10° in the experiment, and the kinematic differential positioning was performed based on the dual-/triple-frequency IF and IR combinations. The Kalman filtering was applied for the parameter estimation. The coordinate parameters were estimated epoch by epoch without any constraint between the epochs. The tropospheric dry component delays of the two stations were corrected by the Saastamoinen model first. The corresponding residual zenith tropospheric wet component delays were estimated for each station using a random walk model with a process noise value of 10^{-4} m/sqrt(s). The

differential ionospheric delay errors were ignored, and the site displacement effect by solid earth tide was corrected by the IERS Conventions model (McCarthy 1996). The ambiguity parameters of the IF and IR phase combinations were estimated as constants without cycle slips. As a result, the parameters to be estimated are three coordinate parameters, two zenith tropospheric delay parameters and ambiguity parameters. Because the wavelength of the IF phase combinations is short, the corresponding ambiguity parameters are estimated in units of distance and the ambiguity parameters of the IR phase combinations are estimated in units of cycles to facilitate the subsequent AR process.

Positioning accuracy and convergence speed

The positioning accuracy of the kinematic differential positioning by the IF and IR phase combination is listed in Table 7. In order to evaluate the improvement of the differential positioning using the triple-frequency IF and IR combinations in terms of convergence speed, a total of 14 convergence processes in 7 days were analyzed by restarting the solutions every 12 h. The average convergence series are presented in Fig. 8.

Table 7 shows that the RMSs of the differential positioning errors, for all the triple-frequency IF and IR combinations, are smaller than those of the dual-frequency combinations. Compared to the dual-frequency IF and IR combinations #8 and #14, the positioning RMSs of the triple-frequency IF and IR combinations #1 and #11 improved by about 7% and 9%, respectively. The positioning errors are shown in Figs. 5 and 6. In addition, the positioning accuracy of the IR combination (#11) is even slightly better than that of the IF combination #14, and their positioning errors are shown in Fig. 7. It demonstrates that even for a baseline length close to 1600 km the differential ionospheric delay error of the IR combinations is still negligible.

Figure 8 shows that the convergence series of the IF and IR combinations are very consistent and the float solution convergence speed of the triple-frequency IF and IR combinations is slightly faster than that of the corresponding dual-frequency IF and IR combinations.

Ambiguity estimation

The float ambiguities of the optimal IR combination #11 were fixed to integer values by the LAMBDA algorithm (Teunissen 1995) directly. The ratio test was used for the acceptance, and the threshold value is taken as 3.0. Since reliable ambiguity fixing of newly rising satellites usually needs some time in case of long baselines (Takasu and Yasuda 2010), a simple partial ambiguity fixing strategy is employed, that is, only the ambiguities of the satellites with enough continuous valid data over a threshold after they first

Table 7 Float solution accuracy of the kinematic differential positioning by the IF and IR phase combinations (unit: cm)

Combinations	Number	Linear coefficients			Urumqi–Lhasa		
					H	V	Position
IF	#1	242	218	−345	5.6	14.6	15.6
	#2	286	327	−460	5.6	14.6	15.6
	#3	198	109	−230	5.7	14.7	15.7
	#4	44	109	−115	5.6	14.8	15.8
	#5	352	109	−345	5.8	14.9	16.0
	#6	506	109	−460	5.9	15.0	16.2
	#7	66	545	−460	5.6	15.3	16.3
	#8	154	0	−115	6.2	15.7	16.8
	#9	22	436	−345	5.7	15.5	16.5
	#10	0	763	−575	5.7	15.7	16.7
IR	#11	2	2	−3	5.3	13.0	14.1
	#12	3	1	−3	5.6	13.4	14.5
	#13	1	3	−3	5.2	13.3	14.2
	#14	4	0	−3	6.0	14.3	15.5
	#15	0	4	−3	5.2	14.1	15.0
Improvement #1 versus #8 (%)					9.7	7.0	7.1
Improvement #11 versus #14 (%)					11.7	9.1	9.0
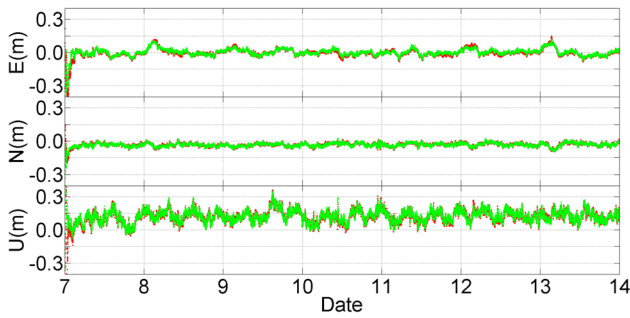
Fig. 5 Float solution errors of differential positioning for both the dual- and triple-frequency IF combinations (red: #8, green: #1)
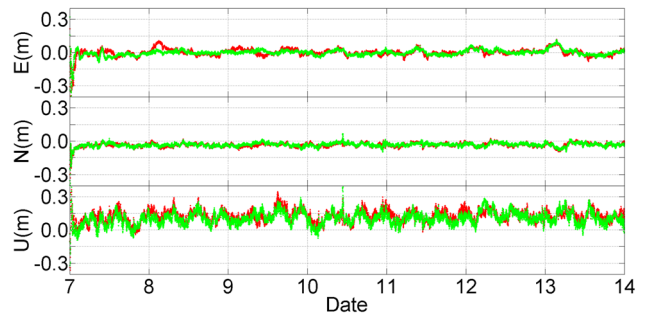
Fig. 7 Float solution errors of differential positioning for the triple-frequency IF and IR combinations (red: #1, green: #11)
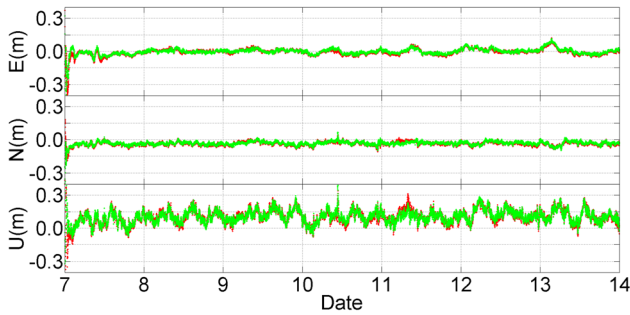

Fig. 6 Float solution errors of the differential positioning for both the dual- and triple-frequency IR combinations (red: #14, green: #11)
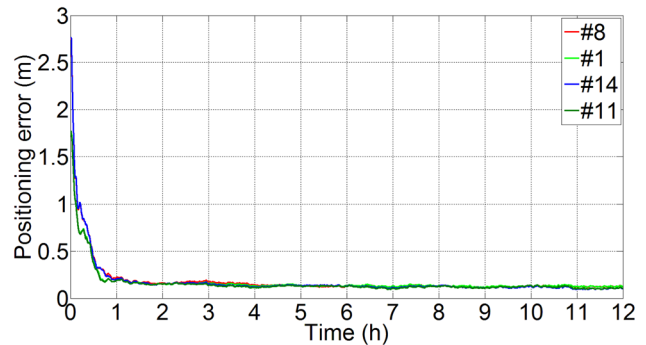

Fig. 8 Average convergence series of the differential positioning by the triple-frequency IF and IR combinations

become visible are resolved to integers. In this experiment, the ambiguity fixed rate reaches 88.4% when the threshold value is set to 120 epochs. The results are shown in Fig. 9.

Figure 9 shows that the fixed solution errors are continuously stable which verifies the feasibility of the IR combined
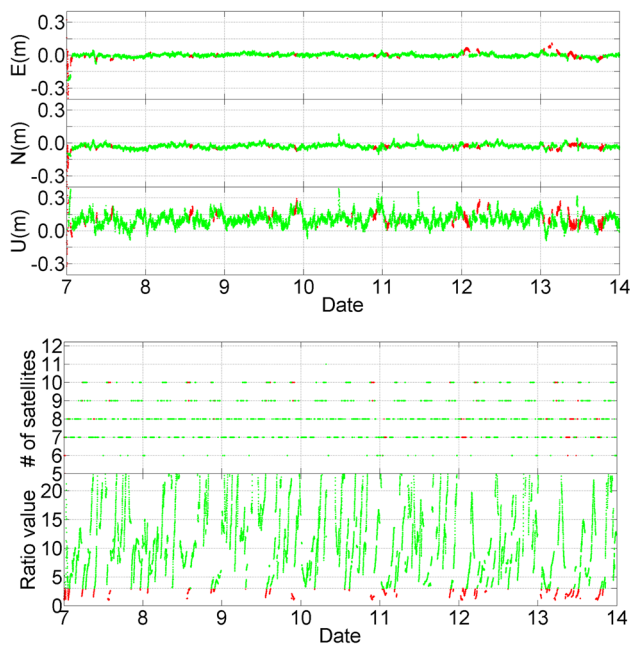
Fig. 9 Positioning errors (top) and ratio values (bottom) of the differential positioning by triple-frequency IR combination (red: float, green: fixed)

ambiguity estimation directly over a long baseline. It is very useful for vehicle positioning at sea (Yang et al. 2018, 2020a).

Conclusions and remarks

BDS-3 system has the most navigation signal frequencies and allows the most frequency combinations among the current GNSS. The triple-frequency linear combinations of the BDS-3 B1C/B1I/B2a signals have remarkable benefits on eliminating or reducing the ionospheric delay errors as well as improving positioning accuracy and ambiguity estimation:

1. Compared to the current best dual-frequency IF and IR combinations of GPS L1/L5 or Galileo E1/E5a, the optimal triple-frequency IF combination $(242, 218, -345)$ and IR combination $(2, 2, -3)$ for the BDS-3 B1C/B1I/B2a signals can improve the measurement accuracy about 20%.
2. In particular, the IR combination $(2, 2, -3)$ with a wavelength of 10.9 cm is almost immune to the ionospheric delay error and has a smaller noise amplification factor compared to the existing dual-frequency IF and IR combinations. Therefore, its combined ambiguities can be fixed directly on the long baseline occasions, which can simplify the current precise positioning process of the IF combination and improve positioning accuracy and AR performance.

3. In real-time kinematic differential positioning applications over long baseline, one needs to transmit two or three code and carrier phase observations to the rover traditionally, but one only needs to transmit a combined IR code observation and a combined IR carrier phase observation. Thus, the phase differential positioning based on the IR combinations can reduce the communication bandwidth by about 43% and 60% in dual- and triple-frequency cases.
4. The presented optimal IR combinations are also very promising for current PPP application due to extremely weak sensitivity to ionospheric delay errors.
5. The frequencies of the B1C/B1I/B2a signals all are in the ARNS band. Therefore, the presented optimal combinations can also be used in safety-of-life applications.

In addition, we note that more frequency combinations require higher consistency between different signals. It can be expected that with the full operational services of BDS-3, the observation model of the BDS-3 signals will continue to be refined, for example, considering phase center offset difference for different signals and possible inter-frequency clock bias (Zhang et al. 2017), and the potential of BDS-3 multi-frequency observations can be further developed.

References

Blewitt G (1989) Carrier phase ambiguity resolution for the global positioning system applied to geodetic baselines up to 2000 km. J Geophys Res 94:10187–10203

Blewitt G (1990) An automatic editing algorithm for GPS data. Geophys Res Lett 17(3):199–202

Cocard M, Bourgon S, Kamali O, Collins P (2008) A systematic investigation of optimal carrier-phase combinations for modernized triple-frequency GPS. J Geod 82(9):555–564

Dong D, Bock Y (1989) Global positioning system network analysis with phase ambiguity resolution applied to crustal deformation studies in California. J Geophys Res 94:3949–3966

Feng Y (2008) GNSS three carrier ambiguity resolution using ionosphere-reduced virtual signals. J Geod 82(12):847–862

Han S, Rizos C (1999) The impact of two additional civilian GPS frequencies on ambiguity resolution strategies. In: Proceedings of ION AM 1999, Institute of Navigation, Cambridge, MA, June 27–30, pp 315–321

Hatch R (2006) A new three-frequency, geometry-free, technique for ambiguity resolution. In: Proceedings of ION GNSS 2006, Institute of Navigation, Fort Worth, TX, USA, September 26–29, pp 309–316

Hatch R, Jung J, Enge P, Pervan B (2000) Civilian GPS: the benefits of the three frequencies. GPS Solut 3(4):1–9

Li J (2014) BDS/GPS multi-frequency real-time precise positioning theory and algorithms (in Chinese). Ph.D. Dissertation, Information Engineering University, Zhengzhou

Li J, Yang Y, He H, Xu J, Guo H (2012) Optimal carrier-phase combinations for triple-frequency GNSS derived from an analytical method (in Chinese). Acta Geodaet Cartograph Sin 41(6):797–803

Li T, Wang J, Laurichesse D (2014) Modeling and quality control for reliable precise point positioning integer ambiguity resolution with GNSS modernization. GPS Solut 18(3):429–442

Li J, Yang Y, Junyi X, He H, Guo H (2015) GNSS multi-carrier fast partial ambiguity resolution strategy tested with real BDS/GPS dual- and triple-frequency observations. GPS Solut 19(5):5–13

Li J, Yang Y, He H, Guo H (2017) An analytical study on the carrier-phase linear combinations for triple-frequency GNSS. J Geod 91(2):151–166

Li B, Qin Y, Liu T (2019) Geometry-based cycle slip and data gap repair for multi-GNSS and multi-frequency observations. J Geod 93(3):399–417

McCarthy DD (1996) IERS technical note 21. IERS conventions 1996. http://iers-conventions.obspm.fr/conventions_archive.php. Accessed 30 July 2020

Odijk D (2003) Ionosphere-free phase combinations for modernized GPS. J Surv Eng 129(4):165–173

Richert T, El-Sheimy N (2007) Optimal linear combinations of triple-frequency carrier phase data from future global navigation satellite systems. GPS Solut 11(1):11–19

RTCM-SC104 (2013) RTCM standard 10403.2 differential GNSS services-version 3. RTCM Special Committee 104, Nov 7 2013. https://rtcm.myshopify.com/collections/differential-global-navigation-satellite-dgnss-standards. Accessed 30 July 2020

RTCM-SC104 (2018) RINEX Receiver independent exchange format version 3.04. Radio Technical Commission for Maritime Services Special Committee 104

Saastamoinen J (1973) Contributions to the theory of atmospheric refraction. Bull Geod 107:13–34

Simsky A (2006) Three's the charm: triple-frequency combinations in future GNSS. Inside GNSS, July/August 2006, pp 38–41

Takasu T, Yasuda A (2010) Kalman-filter-based integer ambiguity resolution strategy for long-baseline RTK with ionosphere and troposphere estimation. In: Proceedings of ION GNSS 2010, Institute of Navigation, Portland, OR, September 21–24, pp 161–171

Teunissen PJG (1995) The least-squares ambiguity decorrelation adjustment: a method for fast GPS integer ambiguity estimation. J Geod 70(1):65–82

Yang YX, Xu TH, Xue SQ (2018) Progresses and prospects in developing marine geodetic datum and marine navigation of China. J Geod Geoinf Sci 1(1):16–24

Yang Y, Gao W, Guo S, Mao Y, Yang Y (2019) Introduction to BeiDou-3 navigation satellite system. Navigation 66(1):7–18

Yang Y, Liu Y, Sun D, Xu T, Xue S, Han Y, Zeng A (2020a) Seafloor geodetic network establishment and key technologies. Sci China Earth Sci. https://doi.org/10.1007/s11430-019-9602-3

Yang Y, Mao Y, Sun B (2020b) Basic performance and future developments of BeiDou global navigation satellite system. Satell Navig 1:1

Zhang X, He X (2015) BDS triple-frequency carrier-phase linear combination models and their characteristics. Sci China Earth Sci 58(6):896–905

Zhang X, Li P (2016) Benefits of the third frequency signal on cycle slip correction. GPS Solut 20(3):451–460

Zhang X, Wu M, Liu W, Li X, Yu S, Lv C, Wickert Y (2017) Initial assessment of the COMPASS/BeiDou-3: new-generation navigation signals. J Geod 91(10):1225–1240

Zhao Q, Sun B, Dai Z, Hu Z, Shi C, Liu J (2015) Real-time detection and repair of cycle slips in triple-frequency GNSS measurements. GPS Solut 19(3):381–391
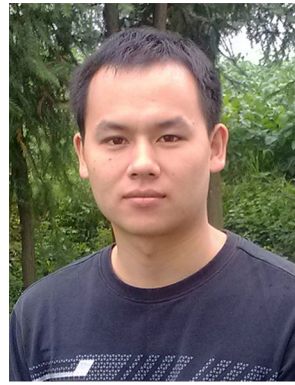
Jinlong Li obtained his Ph.D. degree from Information Engineering University in 2014 and is currently an engineer at Beijing Satellite Navigation Center, China. His current research focuses on multi-frequency GNSS RTK and PPP positioning and satellite-based augmentation systems.

Yuanxi Yang is currently a Professor of Geodesy and Navigation at Xi'an Institute of Surveying and Mapping. He got his Ph.D. from Wuhan Institute of Geodesy and Geophysics of the Chinese Academy of Science. He was honored as an Academic Member of the Chinese Academy of Science in 2007. His research interests mainly include geodetic data processing, geodetic coordinate system, crustal deformation analysis and comprehensive PNT.

Haibo He obtained his Ph.D. degree from Information Engineering University in 2002 and is currently a senior engineer at Beijing Satellite Navigation Center, China. His current research interests include GNSS high-precision positioning and attitude determination.

Hairong Guo obtained her Ph.D. degree from Information Engineering University in 2006 and is currently a senior engineer at Beijing Satellite Navigation Center, China. Her current research mainly involves GNSS high-precision survey and application.